Sand tested under cyclic triaxial conditions with constant radial stress

Sable testé dans des conditions triaxiales cycliques avec contrainte radiale constante

E.F.Cosgrove & B.M.Lehane – *Dept. of Civil Engineering, University of Dublin, Trinity College, Ireland*
C.W.W.Ng – *Dept. of Civil Engineering, Hong Kong University of Science and Technology, China*

ABSTRACT: Drained cyclic triaxial tests were performed on a range of Leighton Buzzard sand samples to assist interpretation of the settlements that take place in backfill adjacent to integral bridge abutments. Specimens were load cycled for a range of constant axial strain amplitudes varying from ±0.05% to ±1% and radial stresses were held constant. The test results reveal characteristics which differ significantly from those observed in the more commonly performed constant cyclic stress ratio tests and constant shear strain amplitude tests.

RÉSUMÉ: Des essais triaxiaux cycliques drainés ont été réalisés sur un ensemble d'échantillons de sable Leighton Buzzard pour aider à l'interprétation des tassements qui ont lieu dans les remblais adjacents aux cufées de pont intégral. Les spécimens étaient chargés cyclequement pour un intervalle d'amplitudes axiales constantes de contrainte changeant de ± 0.05% à ± 1% et d'efforts radiaux constants. Les résultats des essais indiquent que les caractéristiques diffèrent de maniere significative de ceux observées dans les essais généralement realisés à contrainte moyenne constante et avec un taux de contrainte cyclique et dans les essais avec une amplitude de contrainte cisaillement constante.

1 INTRODUCTION

The exclusion of movement joints from within the decks of integral bridges results in significant cyclic displacements of their abutments and consequent progressive settling of the adjacent backfill. In support of physical experiments which measured the settlement of this backfill (detailed in Cosgrove 2001), a series of cyclic triaxial tests were performed to assess the performance of Leighton Buzzard Sand (LBS) under two-way cycling conditions with constant axial strain amplitude and constant radial stress. Findings from these tests are presented and discussed.

2 TESTING PROGRAMME

The LBS tested was imported from the UK and had a mean particle size of 0.12mm and a uniformity coefficient of 1.5. Loose samples were prepared by air pluviation and denser samples were created by light vibration of the pluviated samples. Saturation was assisted using a CO_2 flush and a backpressure of 200kPa was maintained throughout. All triaxial tests considered in this paper involved initial isotropic consolidation of samples to a mean effective stress (p') of 90kPa and subsequent two-way axial strain controlled cyclic loading at constant radial stress, σ_r = 90kPa. The axial strain rate during testing was maintained at 0.066% per minute. Additional experiments involving isotropic cycling were performed to supplement these tests.

3 OVERALL ACCUMULATION OF VOLUMETRIC STRAIN

The variation of the contraction (compressive volumetric strain), ε_v, measured at the end of each cycle with the number of cycles (N) is plotted on Figure 1 for samples cycled with a range of axial strain amplitudes (ε_{amp}) and initial sample relative densities (D_r) (after consolidation). It is apparent that contraction is most significant over the earlier 5 to 10 cycles and that the degree of contraction increases with ε_{amp} and is less significant for denser samples. Supplementary tests involving isotropic loading and unloading of samples (by cycling the cell pressure) from an initial p' value of 90kPa indicated that less than 15% of the total contractions indicated on Figure 1 were brought about by cyclic variations in p'.

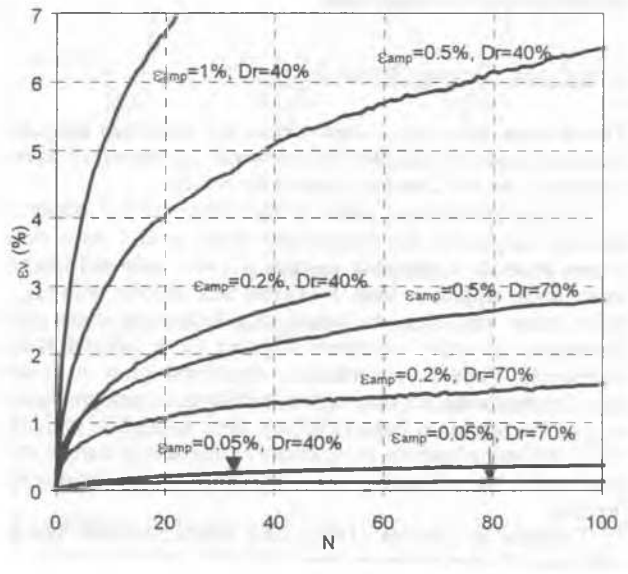

Figure 1. Contraction (compressive volumetric strain) versus the number of cycles.

Byrne & McIntyre (1994) used two-way cyclic simple shear tests on sand to deduce empirical relationships between ε_v and N; these relate an increment of volumetric strain to the shear strain amplitude, sample density and current volumetric strain, as follows:

$$\Delta\varepsilon_{v\,(1/2\ cycle)} = 0.5\,\gamma\,C_1 \exp(-C_2\varepsilon_v / \gamma) \qquad (1)$$

where $\Delta\varepsilon_{v\,(1/2\ cycle)}$ = half cycle volumetric strain increment; γ = shear strain amplitude; ε_v = current volumetric strain and C_1 & C_2 are constants which depend on D_r (C_1 reduces and C_2 increases as D_r increases).

The constants C_1 & C_2 were derived for the tests shown in Figure 1, using Equation 1, and accounting for the reductions in cyclic shear strain amplitude that take place in constant ε_{amp} tests. These values are given in Table 1 alongside Byrne's simple shear constants.

Table 1. Empirical constants to deduce contractions (See Byrne & McIntyre (1994))

Simple shear tests			Cyclic triaxial tests		
D_r(%)	C_1	C_2	D_r(%)	C_1	C_2
34	1	0.4	-	-	-
40	0.72	0.56	40	1.0 ±0.15	0.4 ±0.15
47	0.5	0.8	-	-	-
70	0.19	2.13	70	0.5 ±0.15	0.8 ±0.15

It is evident from Table 1 that, for a given D_r, C_1 values are greater in triaxial tests than the respective values in simple shear tests while C_2 values in the latter exceed those of the triaxial tests. These trends indicate that, at equivalent shear strain amplitudes and densities, contraction in the triaxial tests is higher than in simple shear tests. For example, the coefficients in Table 1 suggest that the degree of contraction experienced by a sample with $D_r \approx 70\%$ in the constant ε_{amp} triaxial tests is similar to that of a sample tested in cyclic simple shear with $D_r \approx 47\%$. The higher contractions in the triaxial tests occur partly because of cyclic p' variations (that do not take place in the simple shear tests). However, the primary reason is due to the fact that samples with $\varepsilon_{amp} \geq 0.2\%$ come close to failure in extension. This causes significant dilation and results in pronounced contraction following reversal of loading direction. These contractions dominate the overall volumetric response resulting in higher contraction than in simple shear.

4 STRESS - STRAIN RESPONSE

The deviator stress (q) - axial strain (ε_a) responses of loose-medium dense LBS samples with constant ε_{amp} values are shown in Figure 2 for N = 2 and in Figure 3 for N = 25.

The non-symmetrical nature of the curves for $\varepsilon_{amp} \geq 0.2\%$ is in sharp contrast to the symmetrical shear stress - shear strain curves generally obtained in constant p' cyclic tests and constant shear strain amplitude tests. It is clear that samples with $\varepsilon_{amp} \geq 0.2\%$ come very close to failure in extension in every cycle (analogous to active conditions adjacent to an integral bridge abutment). There is, nevertheless, significant strain hardening e.g. the maximum deviator stress mobilized in compression at ε_{amp}=1.0% increases from 155kPa at N=2 to 250kPa at N=25. Such hardening leads to an appreciable increase in sample stiffness and a more linear q *vs.* ε_a response during compression loading.

Tatsuoka & Shibuya (1992), and others, confirm that the stiffness of clean siliceous deposits varies approximately with the void ratio function, $F(e) = (2.17\text{-}e)^2/(1+e)$, where e is the void ratio. The equivalent Young's moduli for each cycle, E_{eq} [$= (q_{max}-q_{min})/2\varepsilon_{amp}$] for samples with an initial D_r of $\approx$ 40% are normalized by the current F(e) value and plotted against N on Figure 4.

The observed rise of $E_{eq}/F(e)$ with N is not due to densification but is indicative of a significant increase in stiffness due to structural or fabric changes. Most significant relative increases in $E_{eq}/F(e)$ occurred for initially loose samples with $\varepsilon_{amp} \geq 0.2\%$. The pronounced influence of cyclic straining may be appreciated when one considers that the equivalent stiffness of loose-medium dense LBS at ε_{amp} = 0.2% almost doubled at N=50 while its relative density increased by only 13%.

Hachey & Been (1989) used drained and undrained triaxial tests to establish the steady/critical state line (SSL) for monotonically sheared LBS. This line may be expressed as $\upsilon = 1.026\text{-}0.054\log(p')$, where υ is the specific volume. The monotonic peak envelope (MPE) was also determined and is expressed as $(\phi'_p\text{-}\phi'_{cv}) = -53\ \psi$, where ϕ'_p and ϕ'_{cv} (32°) are the peak and steady state friction angles and ψ is the state parameter defined as the current void ratio less the void ratio at the same p' value on the SSL. This MPE is plotted on Figure 5 and compared with the maximum angles of friction mobilized during all the extension cycles of four separate tests. It is evident that mobilized friction angles increase progressively during cycling and, for $\varepsilon_{amp} \geq 0.2\%$, angles increase to well above those of the MPE. In addition, the sample state moves away from the SSL (ψ=0) towards an end state which varies with the applied ε_{amp} value and the initial state parameter.

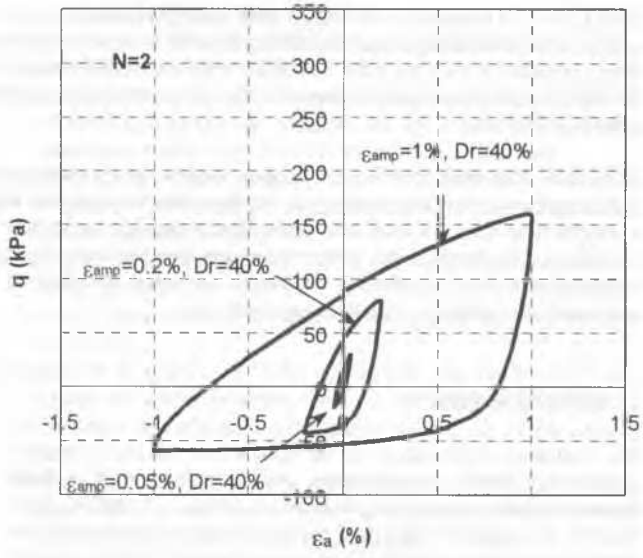

Figure 2. Deviator stress - axial strain (ε_a) response of LBS at N = 2.

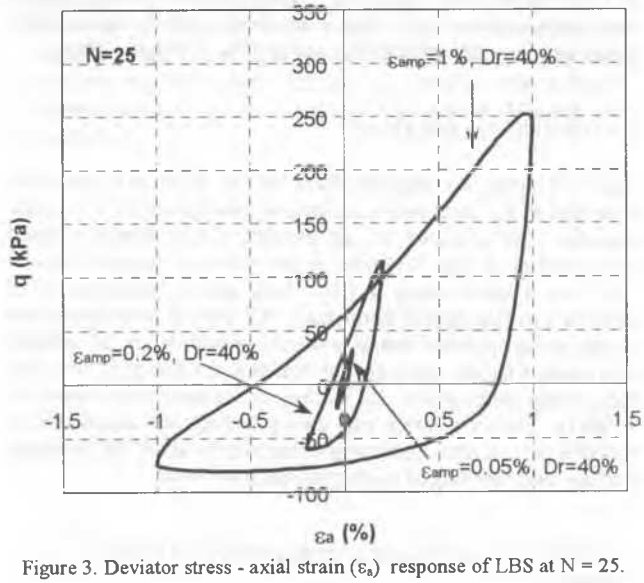

Figure 3. Deviator stress - axial strain (ε_a) response of LBS at N = 25.

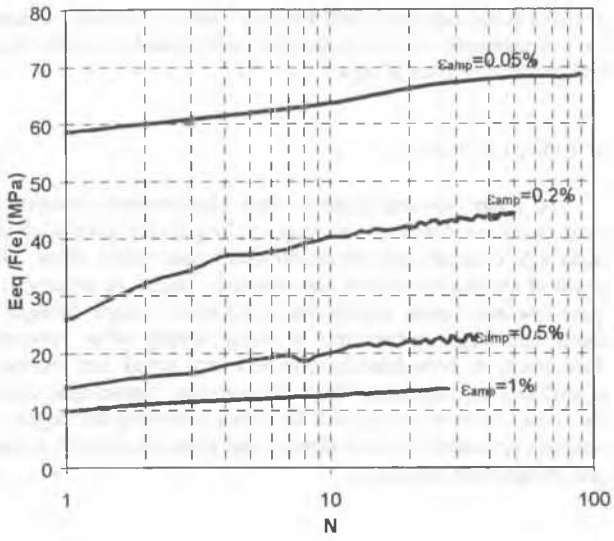

Figure 4. Equivalent Young's modulus (normalized by F(e)) versus number of cycles for loose-medium dense LBS.

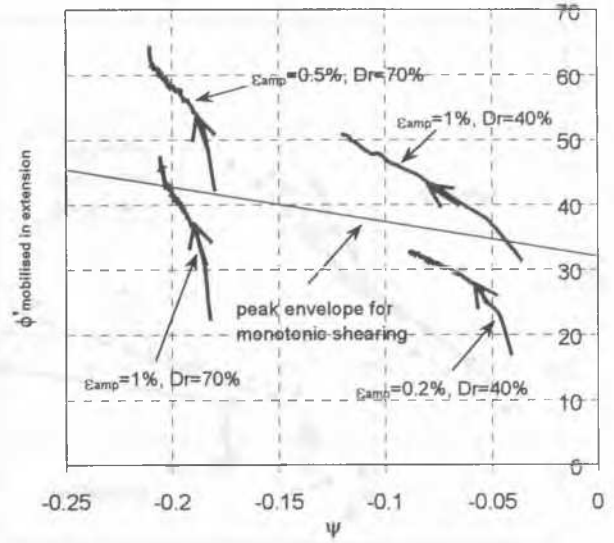

Figure 5. Mobilized friction angle in extension versus the current state parameter.

5 STRESS - DILATANCY RELATIONSHIPS

Stress-dilatancy relationships cannot be established directly from the triaxial tests under consideration as the volume changes due to variations in p' and those due to shear are indistinguishable. However, if samples are assumed to be isotropic and coupling of shear and volumetric components is ignored, approximate trends may be derived using the procedure outlined in Pradhan et al. (1989). This procedure proposes that the volume change due to changes in p' (ε_{vc}) may be assessed from tests on identical samples subjected to isotropic loading and unloading. κ^* (defined in Equation 2) is derived from isotropic cyclic p' tests on loose and dense LBS (membrane penetration effects included) and its variation over a range of cycles for a loose test, with p' cycling between 60kPa to 120kPa, is illustrated in Figure 6. (Note that almost identical κ^*values were found in dense tests).

$$\kappa^* = \delta\varepsilon_v / \ln((p'+\delta p')/p') \quad (2)$$

The measured variation of κ^* during cycling may be represented as:

$$\kappa^* = (\kappa^*_{mean} - \Delta\kappa^*) + 2\Delta\kappa^* N_f \text{ during loading} \quad (3a)$$

$$\kappa^* = (\kappa^*_{mean} + \Delta\kappa^*) - 2\Delta\kappa^* N_f \text{ during unloading} \quad (3b)$$

where $\Delta\kappa^*$ = amplitude of variation in κ^* and N_f is a factor increasing from 0 to 1 during loading or unloading.

Equation 3 is plotted in Figure 6, using the κ^* values given in Table 2.

Table 2. κ^* values from isotropic cyclic p' tests

Loading	Unloading
κ^*_{mean} = 0.00165	κ^*_{mean} = 0.0015
$\Delta\kappa^*$ = 0.00055	$\Delta\kappa^*$ = 0.0004

The volumetric strain increment due to shear ($d\varepsilon_{vd}$) may then be estimated by subtracting the $d\varepsilon_{vc}$ calculated using Equations 2 and 3 from the measured total volumetric strain increment.

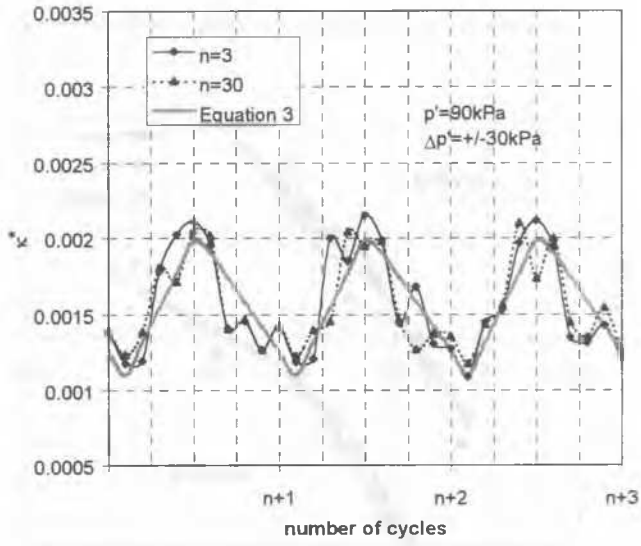

Figure 6. Variation of κ^* during isotropic cyclic p' tests.

Cosgrove (2001) shows that the small-strain elastic vertical Young's modulus of LBS, E_{V0}, can be represented as:

$$E_{v0}\,(MPa) = 220\,F(e)\,(\sigma'_v/p_a)^{0.5} \quad (4)$$

where F(e) is the void ratio function (as defined), σ'_v is the current vertical effective stress and p_a is atmospheric pressure (= 100kPa). If a small-strain Poisson's ratio, ν_0, of 0.1 is adopted, elastic shear strain increments ($d\gamma_e$) may be deduced using Equation (4) and consequently plastic shear strain increments ($d\gamma_p$) are obtained by subtracting $d\gamma_e$ from the measured total shear strain increment.

The dilatancy rate, $D = d\varepsilon_{vd}/d\gamma_p$, was calculated in the manner described and its variations with $\eta = q/p'$ in tests on loose and dense samples with ε_{amp}= 0.2% are plotted on Figures 7 and 8 for cycles numbers 3, 10 and 30. In general and, as predicted by Rowe's stress dilatancy theory, D is seen to vary in an approximate linear fashion with η. There is, however, a far less linear and more erratic response on unloading of the loose sample, par-

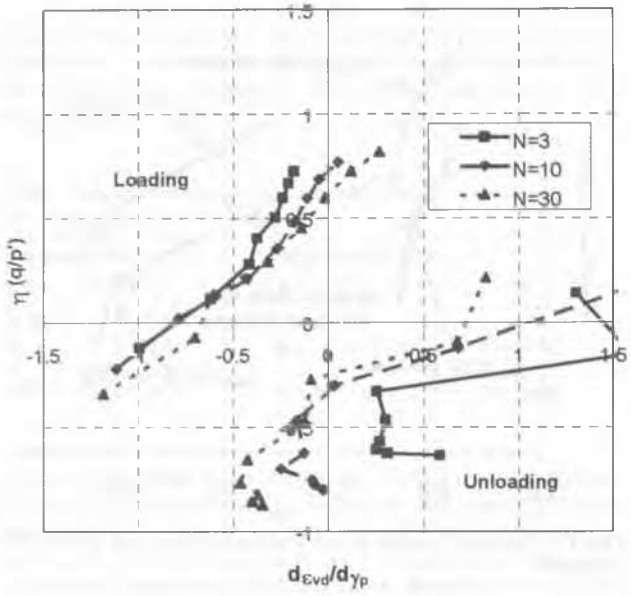

Figure 7. η versus dilatancy rate $D = d\varepsilon_{vd}/d\gamma_p$ ($D_r \approx 40\%$)

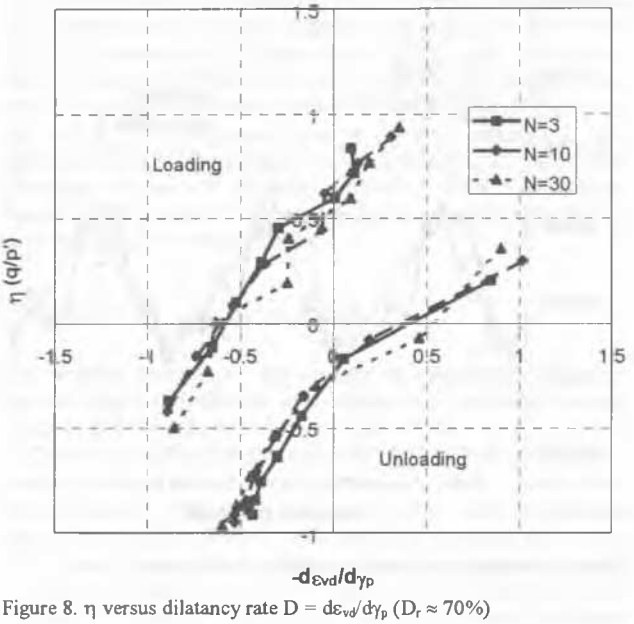

Figure 8. η versus dilatancy rate $D = d\varepsilon_{vd}/d\gamma_p$ ($D_r \approx 70\%$)

ticularly at low N values. A 'hook' in the dilatancy rate is observed towards the end of unloading of the loose test, which does not occur in the test on the dense sample. Similar characteristics are presented by Wan & Guo (1999) during monotonic shearing. It is also clear from Figures 7 and 8 that a reduction of η at D = 0 (η_0) occurs during cycling, particularly for the loose test, while the slope of D vs. η is relatively constant. η_0 continues to decrease as long as there is net contraction within a cycle.

Based on monotonic and cyclic triaxial tests reported in Pradhan et al. (1989), η_0 in extension ≈ 0.6-1 times η_0 in compression. From Figures 7 and 8 it is clear that η_0 during unloading is much less than that found by Pradhan et al. This may be partly attributed to the approximate technique employed to derive Figures 7 and 8 but is also likely to be due to the proximity of the samples to failure in extension compared with compression. During reloading after extension, large contractions dominate as the material reaches its densest state, and significant strain hardening occurs. While some dilation begins towards the end of loading (see Figs 7 and 8), it is insufficient to destroy the dense fabric formed during loading. As a result, during unloading, the initial contraction turns to dilation after a relatively small change in stress ratio compared with loading. Hence, η_0 during unloading is considerably less that that normally found in cyclic stress ratio/cyclic shear strain tests.

6 CONCLUSIONS

The paper has highlighted some characteristic features of clean sand subjected to two-way cycling under triaxial conditions with constant axial strain amplitude and radial stress. This mode of cycling brings the sand close to failure in extension at quite low axial strain amplitudes which allows major changes in fabric and large contractions to occur during stress reversals. This results in both densification and very significant increases in stiffness and strength. These increases are higher than anticipated and have to be allowed for when assessing the degree of restraint provided by the abutment and adjacent backfill to integral bridge deck expansion.

REFERENCES

Byrne, P.M. & McIntyre, J. 1994. Deformations in granular soils due to cyclic loading. Geotechnical Special Publication, American Society o Civil Engineers. 2 (40):1864-1896.

Cosgrove, E.F. 2001. *Cyclic loading of soils behind integral bridge abutments*. PhD Thesis. Trinity College Dublin.

Hachey, J.E. & Been, K. 1989. *Laboratory testing of Leighton Buzzard 120/5 sand*. Golder Associates Ltd., Consulting Engineers, Alberta, Calgary. Report 882-2068.

Pradhan, T. B.S., Tatsuoka, F., & Sato, Y. 1989. Experimental stress-dilatancy relations of sand subjected to cyclic loading. *Soils and Foundations*, Japanese Society of Soil Mechanics and Foundation Engineering, 29(1):45-64.

Tatsuoka, F. & Shibuya, S. 1992. Deformation characteristics of soils and rocks from field and laboratory tests. *Proceedings of the 9th Asian Regional Conference on Soil Mechanics and Foundation Engineering*, Bangkok, 2:101-170.

Wan, R.G. & Guo, P.J. 1999. A pressure density dependent model for granular materials. *Soils and Foundations*, Japanese Society of Soil Mechanics and Foundation Engineering, 39(6):1-11.